© 2022. Published by The Company of Biologists Ltd | Development (2022) 149, dev200495. doi:10.1242/dev.200495

mBeRFP: a versatile fluorescent tool to enhance multichannel live imaging and its applications

Emmanuel Martin* and Magali Suzanne

ABSTRACT

Cell and developmental biology increasingly require live imaging of protein dynamics in cells, tissues or living organisms. Thanks to the discovery and development of a panel of fluorescent proteins over the last decades, live imaging has become a powerful and commonly used approach. However, multicolor live imaging remains challenging. The generation of long Stokes shift red fluorescent proteins offers interesting new perspectives to bypass this limitation. Here, we provide a detailed characterization of mBeRFP for *in vivo* live imaging and its applications in *Drosophila*. Briefly, we show that a single illumination source is sufficient to stimulate mBeRFP and GFP simultaneously. We demonstrate that mBeRFP can be easily combined with classical green and red fluorescent proteins without any crosstalk. We also show that the low photobleaching of mBeRFP is suitable for live imaging, and that this protein can be used for quantitative applications, such as FRAP or laser ablation. Finally, we believe that this fluorescent protein, with the set of new possibilities it offers, constitutes an important tool for cell, developmental and mechano-biologists in their current research.

KEY WORDS: mBeRFP, Fluorescent protein, Live imaging, FRAP, Laser ablation, *Drosophila*

INTRODUCTION

The field of cell and developmental biology relies more and more on the analysis of protein dynamics in cells, tissues or organisms using live imaging. In addition to major advances in fluorescence microscopy, the discovery of the green fluorescent protein (GFP) in the jellyfish *Aequorea victoria* (Shimomura et al., 1962) and its first use as a fluorescent marker in non-jellyfish organisms (Chalfie et al., 1994) were a crucial breakthrough for the field of non-invasive protein imaging. Since the discovery of GFP, many other fluorescent proteins (FPs) have been identified, developed and enhanced, providing a powerful toolkit for visualization of dynamic processes *in vivo* (Chudakov et al., 2010). However, in classical fluorescence imaging, i.e. without a spectral detector and linear unmixing, the number of FPs that can be tracked in a living tissue is often limited by the intrinsic spectral properties of FPs, as well as by the instrumentation available. Indeed, to detect specifically two FPs simultaneously, their excitation and emission peak should be separated by at least 60 nm (Thorn, 2017), so usually only the pairs cyan fluorescent protein (CFP)/yellow fluorescent protein (YFP), or the commonly used GFP/red fluorescent protein (RFP) are imaged together. In some cases, with an adapted set of filters, a third color can be added with little crosstalk, such as RFP with the couple CFP/YFP (Boulina et al., 2013), or blue fluorescent protein (BFP) (mTagBFP2; Subach et al., 2011) with GFP/RFP. However, in this latter case, near-UV excitation is required, which is highly phototoxic for long-term live-imaging experiments (Gorgidze et al., 1998; Icha et al., 2017). Thus, combining more than two colors for live imaging with low phototoxicity, sufficient brightness and photostability of FPs appears challenging, especially in model organisms in which the environment differs greatly from assessments performed *in vitro* to characterize the properties of these FPs (Heppert et al., 2016; Wiedenmann et al., 2009).

During the last two decades, an interest in monomeric red FPs characterized by a large Stokes shift (LSS RFP, i.e. a difference between the emission peak and the excitation peak larger than 150 nm) appeared. These proteins are particularly interesting because they can be excited by blue light, allowing the simultaneous excitation of the LSS RFP with CFP or GFP. Among these LSS RFP, mKeima (Kogure et al., 2006), LSSmKate1, LSSmKate2 (Piatkevich et al., 2010a,b) and mBeRFP (Yang et al., 2013) were generated. However, their full potential in living organisms has not yet been tested.

Here, we provide a detailed characterization of mBeRFP for *in vivo* live-imaging applications in *Drosophila*. First, we cloned and expressed in flies mBeRFP, and showed that it can be easily combined with green and red FPs without crosstalk. We demonstrate that mBeRFP can be combined with enhanced GFP (eGFP) in live imaging, offering the interesting possibility of imaging the two fluorophores using a single light source. We also discuss the potential uses of this protein for quantitative and biophysical applications.

RESULTS AND DISCUSSION

A set of mBeRFP-expressing vectors

To test the potential of fluorescent extended Stokes shift proteins in *Drosophila*, we constructed a set of plasmids expressing either cytoplasmic or nuclear mBeRFP under the control of a UAS promoter (Fig. 1A), as well as a cytoplasmic LSSmKate2, and generated the corresponding transgenic flies. We expressed these constructs using different Gal4 promoters (Fig. 1B,C; Fig. S1A-C) and showed that, at the same laser power, the fluorescence intensity of the LSSmKate2 was not as high as that of mBeRFP (Fig. S1C,D), so we focused on mBeRFP. Then, to ensure that the expression of mBeRFP did not induce developmental defects or cytotoxicity, we followed tissue elongation in pupal leg disk expressing or not expressing cytoplasmic mBeRFP. This revealed that morphogenesis was not affected by the expression of mBeRFP, as shown by the

Molecular Cellular and Developmental Biology (MCD), Centre de Biologie Intégrative (CBI), Université de Toulouse, CNRS, UPS, 31000 Toulouse, France.

*Author for correspondence (martin.emmanuel1987@gmail.com)

E.M., 0000-0003-3878-8633; M.S., 0000-0003-0801-3706

Handling Editor: Thomas Lecuit
Received 3 January 2022; Accepted 12 July 2022

Development (2022) 149, dev200495. doi:10.1242/dev.200495

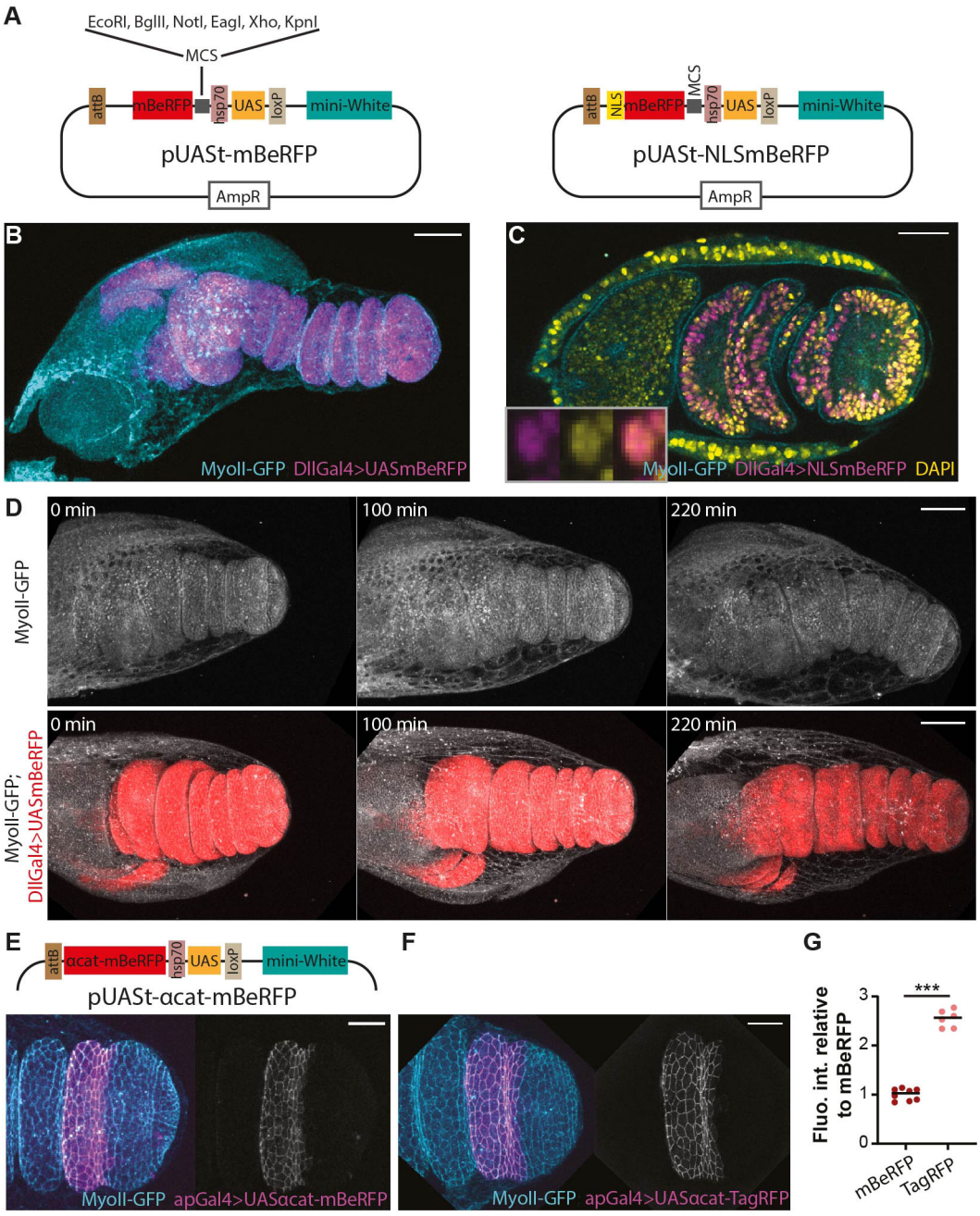

Fig. 1. mBeRFP-expressing vectors for *Drosophila*. (A) The key features of mBeRFP vectors. The restriction sites available in the multiple cloning site (MCS) are listed only once but are the same for all constructs. (B) *z*-projection of an imaginal leg disk expressing endogenous MyoII-GFP (cyan) and cytoplasmic mBeRFP (magenta) in the Dll expression domain. (C) Cross-section of leg epithelium showing the expression of nuclear mBeRFP (magenta) in the Dll expression domain and MyoII-GFP (cyan), stained with DAPI (yellow). Inset shows a zoomed image of a nucleus. (D) Time-lapse images showing the development of MyoII-GFP- and MyoII-GFP; DllGal4>UAS-mBeRFP-expressing legs. (E,F) Distal part of leg epithelium expressing MyoII-GFP (cyan) and UAS-alpha-catenin-mBeRFP (E, magenta/gray) or UAS-alpha-catenin-TagRFP (F, magenta/gray) in the apterous expression domain. In E, the alpha-catenin-mBeRFP vector is schematized. (G) Dot plot representing the fluorescence intensity of mBeRFP and TagRFP relative to the mean fluorescence of all mBeRFP-expressing legs (*n*=8, 6, respectively). Black lines indicate the median. ***P<0.001 (Student's *t*-test). Scale bars: 50 µm (D); 40 µm (B,C); 20 µm (E,F).

normal elongation of the leg and the correct formation of the folds (Fig. 1D; Movie 1).

We then tested the possibility of using mBeRFP as a tag to follow endogenous protein. As a proof of concept, we generated an α-catenin-mBeRFP fusion protein and used α-catenin-TagRFP as a control. Although mBeRFP was less fluorescent than TagRFP when imaged using a similar laser power on fixed samples (Fig. 1G), no significant difference in terms of location and morphogenesis was observed between these two fusion proteins (Fig. 1E,F). These data suggest that mBeRFP could be used *in vivo* in *Drosophila*. In addition, we developed 'promoter-free' versions of mBeRFP (Fig. S1E).

mBeRFP for live imaging

To investigate the possibility of using mBeRFP for live imaging, we determine whether (1) it can be detected at low laser power to ensure tissue viability, (2) it does not affect the dynamics of protein of interest and (3) it is not too sensitive to photobleaching. To check

Development (2022) 149, dev200495. doi:10.1242/dev.200495

these characteristics, we used the α-catenin-mBeRFP fusion protein. We first followed the adherens junction dynamics in the apterous domain during the leg development (Fig. 2A; Movie 2). At large scale, tissue dynamics appeared unperturbed all along the movie. At a cellular scale, we were able to follow the extrusion of apoptotic cells from the apical surface of the leg disk (Fig. 2A′), with a duration similar to our previous observations (Schott et al., 2017). This showed that mBeRFP could be efficiently detected and used to follow dynamic processes in living samples.

Then, we assessed the impact of the mBeRFP fusion on protein dynamics by performing fluorescence recovery after photobleaching (FRAP) experiments on α-catenin fused to mBeRFP, TagRFP or GFP (Fig. 2B-E). This technique allows the kinetics of diffusion of a protein of interest to be evaluated by monitoring the recovery of fluorescent signal following photobleaching. FRAP on α-catenin-mBeRFP junctions indicated that the mobile fraction and the half time recovery were not significantly different from those of α-catenin-TagRFP or α-catenin-GFP, suggesting that the protein dynamics is mainly unaffected by the fusion of mBeRFP. Of note, the mobile fraction of α-catenin-TagRFP was significantly lower than that of α-catenin-GFP.

Next, to address the question of photobleaching, we imaged wing disks expressing α-catenin-GFP and α-catenin-mBeRFP and measured the fluorescence intensity at each time frame, when

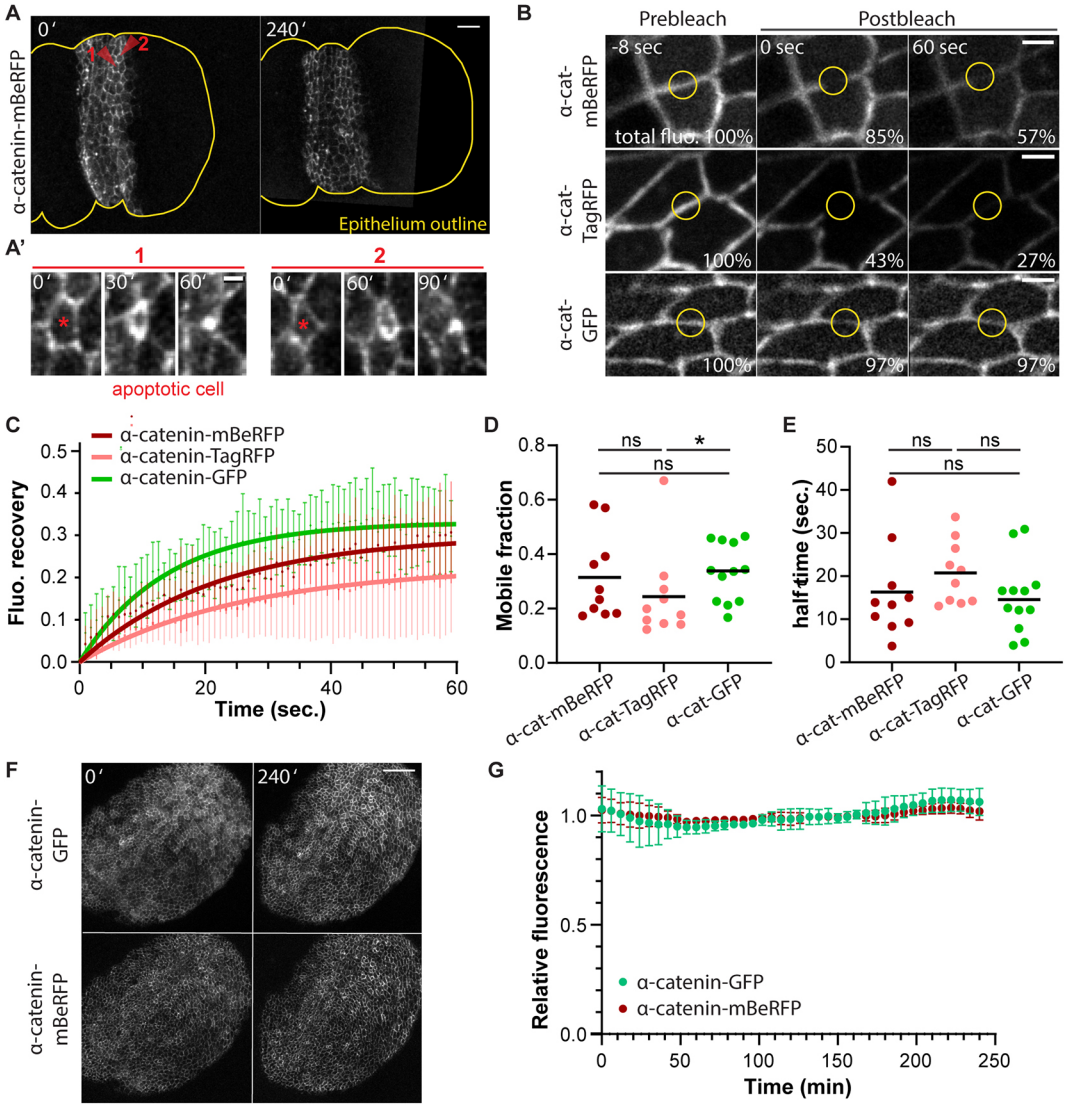

Fig. 2. mBeRFP is a useful protein for live imaging. (A,A′) Time-lapse images of a leg imaginal disk. (A) *z*-projection of the distal part of a leg disk expressing ap-Gal4>UAS-alpha-catenin-mBeRFP at t0 and 4 h after. The yellow line shows the outline of the epithelium. (A′) Enlargements of the two apoptotic cells indicated by red arrowheads in A. Asterisks indicate apoptotic cells at the initial time point. (B-E) mBeRFP-fused protein dynamics. (B) Confocal images showing the fluorescence recovery of alpha-catenin-mBeRFP, alpha-catenin-TagRFP and alpha-catenin-GFP after photobleaching of the ROI (yellow circle) in ap-Gal4, UAS-alpha-catenin-mBeRFP, TagRFP or GFP leg disks. The value at the bottom right of each image indicates the fluorescence of the entire image relative to the prebleach. (C-E) Scatter plots showing the fluorescence recovery over time (C), the mobile fraction (D) and the half time (E) of alpha-catenin-mBeRFP, alpha-catenin-TagRFP and alpha-catenin-GFP in the ROI (n=10, 10, 12, respectively). In C, data represent mean±s.d. and solid lines represent the fitting curves. In D,E, black lines indicate the median. ns, not significant; *P<0.05 (Student's t-test). (F,G) Photobleaching of mBeRFP compared with GFP. (F) Time-lapse images of a wing disk expressing UAS-alpha-catenin-GFP and UAS-alpha-catenin-mBeRFP in the pdm2 expression domain. (G) Fluorescence decay of mBeRFP and GFP measured from live experiments on wing disks (n=3), upon 458 nm laser source excitation. Data represent mean±s.e.m. Scale bars: 10 µm (A); 2 µm (A′,B); 20 µm (F).

Development (2022) 149, dev200495. doi:10.1242/dev.200495

excited with a 458 nm laser (Fig. 2F,G). In this experiment, the fluorescence of both α-catenin-GFP and α-catenin-mBeRFP was stable over time. The same experiment was carried out with wings expressing both E-cadherin-GFP and nuclear mBeRFP with the same result (Fig. S2; Movie 3), providing reassuring evidence that this fluorescent protein can be used for live imaging.

mBeRFP can be combined with green and red FPs without crosstalk

To ensure that mBeRFP can be used in combination with classical FPs, we analyzed the extent of crosstalk in fixed tissues under optimal conditions for fluorescence detection. To test the combination with green-emitting FPs, we used eGFP. Theoretically, eGFP and mBeRFP can be coupled without crosstalk using adapted emission windows (Fig. 3A). In practice, we fixed emission windows from 490 nm to 550 nm for eGFP and from 600 nm to 700 nm for mBeRFP (Fig. 3A). Although the maximal excitation wavelength differs between these two proteins, the higher brightness of eGFP compared with mBeRFP (Thorn, 2017) offers the interesting possibility of exciting the two proteins with the same wavelength. Indeed, at 458 nm wavelength we could excite mBeRFP to more than 90% and eGFP to 60% (Fig. 3A). Then, we imaged at the same time α-catenin-mBeRFP and MyoII-GFP using either a classical confocal mode or a spectral mode to completely avoid potential spectral fluorescence overlap and crosstalk (Fig. 3B) (Zimmermann et al., 2003). The crosstalk measurement revealed a total absence of crosstalk between eGFP and mBeRFP with these settings (Fig. 3C), confirming the possible combination of these two proteins. To test the potential impact of the presence of mBeRFP on GFP fluorescence, we measured the fluorescence of the MyoII-GFP inside or outside the expression domain of α-catenin-mBeRFP. We observed no difference between the two domains (Fig. 3D,E), suggesting that the presence of mBeRFP does not affect GFP fluorescence. To test further the specificity and precision in terms of spatial distribution of the two fusion proteins eGFP and mBeRFP using a single excitation wavelength, we used random illumination microscopy. This newly developed super-resolution technique offers the possibility of achieving unprecedented spatial resolution (around 100 nm) in living tissues (Mangeat et al., 2021). We concomitantly imaged MyoII-GFP and α-catenin-mBeRFP with a single illumination source at 445 nm and were able to resolve distinctly the two cortical myosin belts of neighboring cells separated by the adherens junctions (Fig. S3A,B).

We also tested the possibility of combining mBeRFP with red-emitting FPs. To do so, we compared the emission rate of mBeRFP and TagRFP when excited at 561 nm (Fig. 3A). We imaged leg disks expressing either α-catenin-TagRFP or α-catenin-mBeRFP and compared the fluorescence intensity outside and inside the expression domain (Fig. 3F). As expected, the fluorescence intensity of α-catenin-TagRFP was high inside the expression domain while the fluorescence intensity of α-catenin-mBeRFP was very close to the background intensity. We noted, however, a significant residual collection of fluorescence that could be the consequence of the existence of a second excitation peak of the mBeRFP protein at 580 nm, as characterized from purified protein (Yang et al., 2013). To extend this analysis, we measured the crosstalk between mBeRFP and TRITC dye after fixation of α-catenin-mBeRFP-expressing leg and staining for actin with phalloidin-TRITC. Similar to the eGFP/mBeRFP pair, we imaged the mBeRFP/TRITC pair using either spectral or classical mode when the sample was illuminated with a 561 nm light source. The analysis of the spectral contamination revealed an absence of crosstalk between mBeRFP and TRITC for the settings used in this assay (Fig. S3C,D). Thus, although mBeRFP can be weakly excited at 561 nm, its emission between 570 and 700 nm is close to the background when the laser power is low, suggesting that this fluorescent protein can be easily coupled with red-emitting FPs without disrupting either the observation or the quantification.

In summary, these data showed that mBeRFP can be combined with green or red-emitting FPs or dyes without crosstalk. In addition, this tool could even allow the detection of five distinct channels using four light sources and only three tracks in classical confocal mode (Fig. 3G).

Live imaging and micromanipulation experiments using α-catenin-mBeRFP and MyoII-GFP

In the following experiments, we chose to focus on the acto-myosin cytoskeleton (MyoII-GFP) together with the adherens junctions (α-catenin-mBeRFP), two very dynamic markers, as an example of simultaneous evaluation of tissue mechanics and cell shape changes, a central interest in the field of mechanobiology. Our aim was to show that this new tool could be of interest for long-term, live-imaging experiments and could be combined easily with other markers. We followed cell division in larval wing disk and confirmed that mBeRFP can be easily combined with GFP-fused protein for live imaging (Fig. 4A; Movie 4). Moreover, using the mBeRFP/GFP pair with a single excitation source rather than the GFP/RFP pair using two different lasers sequentially could (1) greatly reduce phototoxicity because the samples are illuminated at a single wavelength (instead of two different wavelengths) and (2) reduce twice the acquisition time, a crucial parameter for studying protein dynamics.

For FRAP experiments, we decided to bleach these proteins at the level of adherens junctions and followed the fluorescence recovery over time. As expected, we observed a higher stability of the adherens junction protein α-catenin compared with myosin (Fig. 4B; Movie 5) and found approximately the same rate of mobile fraction described in other systems (67% compared with 68% and 25% compared with 22%, respectively for MyoII and α-catenin; Kasza et al., 2014; Yonemura et al., 2010). For laser ablation, in the example shown in Fig. 4C and Movie 6, we were able to follow both the vertex displacement, based on the α-catenin-mBeRFP signal, and the fluorescence intensity of myosin at the same time. This showed that after ablation there is a relaxation of the junction, as expected, followed by a step in which the vertices come together concomitantly with a strong accumulation of myosin at the level of the cut (Fig. 4C′,C″), suggesting the establishment of a myosin-dependent repair mechanism, similarly to what has been observed during wound repair (Antunes et al., 2013; Zulueta-Coarasa and Fernandez-Gonzalez, 2018).

Further possibilities of mBeRFP

To summarize, we have shown that mBeRFP can be easily used with low photobleaching and combined with classical FPs, such as GFP and RFP, for multiple applications including long-term live imaging and opto-manipulations. Moreover, the fluorescence of this protein is not disrupted by the fixation protocol (Fig. 3G), allowing imaging of an additional channel in fixed tissue, and making this FP a versatile tool for imaging in model organisms. Additionally, the combination of mBeRFP with GFP allows the study of two distinct proteins of interest using the same illumination source. A single illumination source rather than two could be potentially less deleterious for tissues in terms of phototoxicity, even if this last

Development (2022) 149, dev200495. doi:10.1242/dev.200495

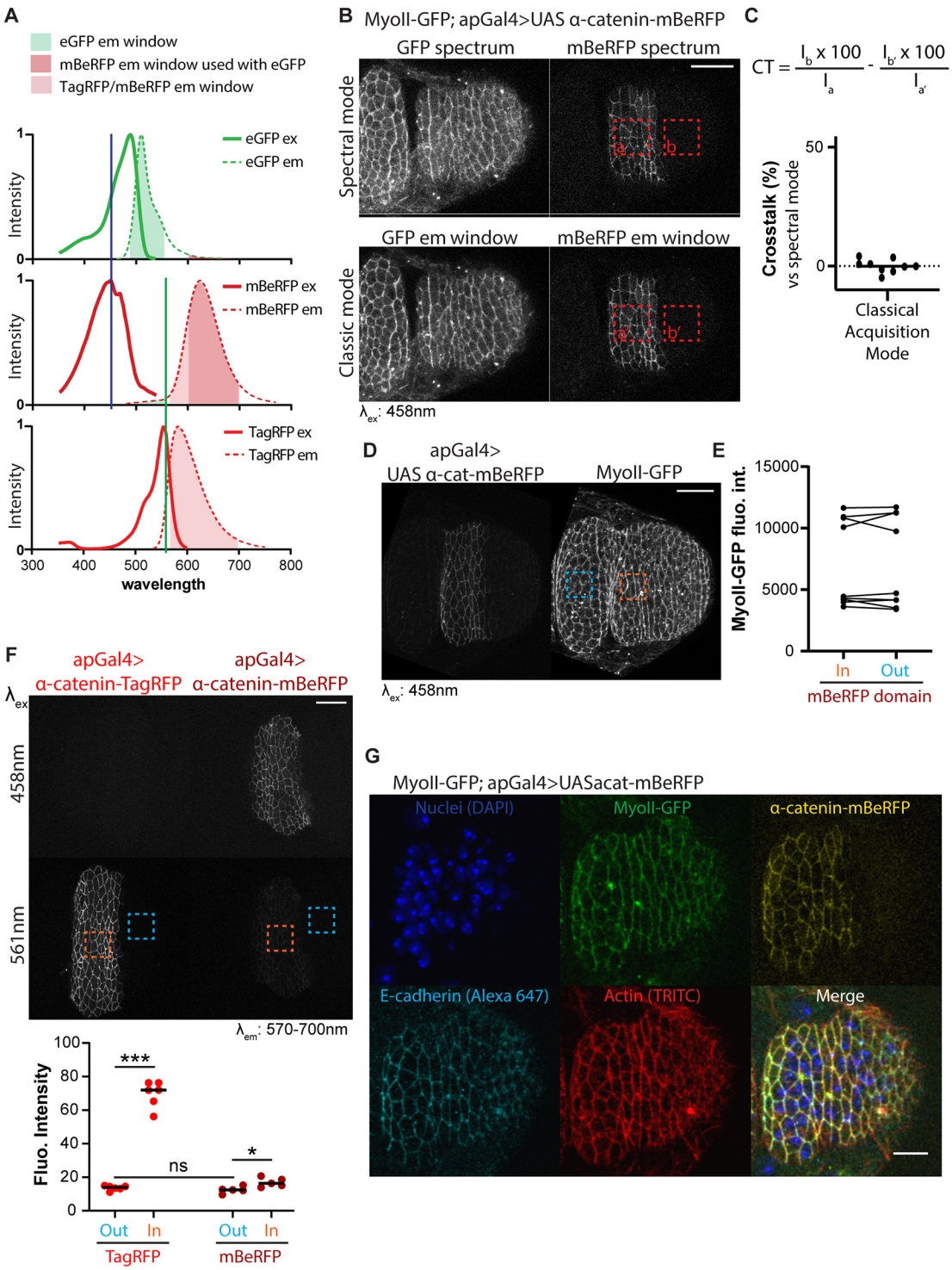

Fig. 3. mBeRFP can be combined with green- and red-emitting fluorescent proteins without any crosstalk. (A) eGFP, mBeRFP and TagRFP excitation and emission spectra showing their respective emission windows (490 to 550 nm, 600 to 700 nm and 570 to 700 nm) and excitation wavelengths used (dark blue line, 458 nm; green line, 561 nm). (B,C) Crosstalk between eGFP and mBeRFP. (B) *z*-projection of the distal part of a leg disk showing MyoII-GFP and UAS-alpha-catenin-mBeRFP imaged using spectral or classical confocal mode. Dashed squares point out areas used to calculate the crosstalk in C. (C) Dot plot representing the crosstalk (CT) together with the corresponding formula (*n*=9). (D,E) Impact of mBeRFP expression on GFP fluorescence. (D) *z*-projection of the distal part of a leg disk showing MyoII-GFP and UAS-alpha-catenin-mBeRFP. (E) Dot plot representing the fluorescence intensity of MyoII-GFP inside and outside the expression domain of alpha-catenin-mBeRFP. Values 'In' and 'Out' are paired for each leg (*n*=9). (F) Emission of TagRFP and mBeRFP in the 570-700 nm emission window when excited at the same power with 458 nm or 561 nm illumination sources. Top: *z*-projection of the distal part of a leg disk showing the emission of UAS-alpha-catenin-TagRFP or UAS-alpha-catenin-mBeRFP. Orange and blue dashed squares point out, respectively, inside and outside areas used to measure the fluorescence intensity. Bottom: Dot plot representing the fluorescence intensity in each zone. *n*=6 and 5 for alpha-catenin-TagRFP and alpha-catenin-mBeRFP, respectively. Black lines indicate the median. ns, not significant; **P*<0.05; ****P*<0.001 (Student's *t*-test). (G) Five-color *z*-projection of the distal part of a leg disk showing nuclei (DAPI; blue), MyoII-GFP (green), and UAS-alpha-catenin-mBeRFP expressed in the apterous domain (yellow), E-cadherin (cyan) and actin (phalloidin; red). Scale bars: 20 µm (B,D,F); 10 µm (G).

Development (2022) 149, dev200495. doi:10.1242/dev.200495

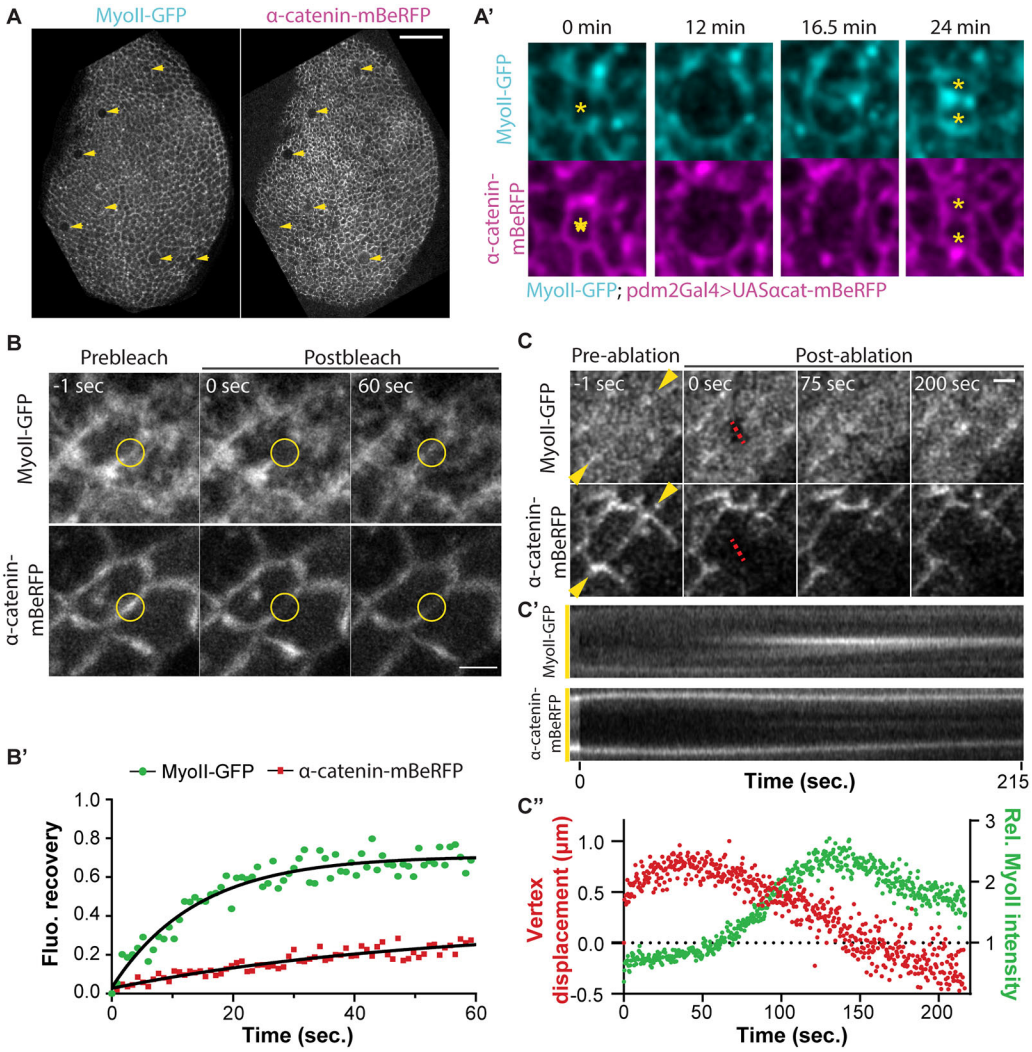

Fig. 4. α-Catenin-mBeRFP and MyoII-GFP combination for live imaging and micromanipulation experiments. (A-A′) Live imaging of cell division. (A) Confocal images of a wing disk expressing MyoII-GFP; pdm2Gal4>UAS-alpha-catenin-mBeRFP, and highlighting cell divisions (yellow arrowheads). (A′) Time-lapse images of a divided cell (asterisks) from the wing disk shown in A. (B,B′) FRAP experiment. (B) Confocal images showing the fluorescence recovery of alpha-catenin-mBeRFP and MyoII-GFP after photobleaching of the ROI (yellow circle) in a MyoII-GFP; ap-Gal4>UAS-alpha-catenin-mBeRFP leg disk. (B′) Scatter plot showing the fluorescence recovery over time of MyoII-GFP and alpha-catenin-mBeRFP in the ROI. Graph shows one representative experiment (*n*=5). Black lines represent the fitting curves. (C-C″) Laser-ablation experiment. (C) Confocal images showing the dynamics of adherens junctions and MyoII before and after laser ablation (red dashed line) in a MyoII-GFP; ap-Gal4>UAS-alpha-catenin-mBeRFP leg disk. (C′) Kymograph of adherens junctions and MyoII at the level of the yellow arrowheads. (C″) Scatter plots showing both the vertex displacement (red) and the fluorescence intensity of the MyoII at the level of the cut (green) over time. Graph shows one representative experiment (*n*=7). Scale bars: 20 µm (A); 2 µm (B,C).

property depends on the wavelength used as well as several other parameters (Icha et al., 2017).

If we consider excitation and emission spectra, mBeRFP could also be coupled with CFP, allowing both proteins to be excited together using a single light source, as previously shown (Yang et al., 2013), and YFP family proteins. Thus, it would potentially be possible to combine the most popular FRET pair – CFP/YFP (Bajar et al., 2016) – with an additional marker coupled to mBeRFP and image them simultaneously using a single illumination source at 458 nm.

Furthermore, considering how close the mBeRFP excitation spectrum is to those of CFP and GFP, we hypothesized that mBeRFP and GFP could be simultaneously observed using multiphoton microscopy, as similarly shown for CFP and GFP (Sahai et al., 2005), although it should offer better detection of each FP. Similarly, it has previously been shown that LSSmKate1, a mBeRFP sister protein, can be combined and simultaneously excited at an optimal wavelength (870 nm) with CFP and GFP for multicolor imaging using two-photon microscopy (Piatkevich et al., 2010a).

Overall, considering the possibility of easily combining mBeRFP with other FPs, its relatively high brightness and stability in living tissues, the wide number of potential applications for live imaging as well as the possibility of using it on fixed tissues, we strongly believe that this fluorescent protein and the versatile constructs we generated will constitute important tools for cell, developmental and mechano-biologists in their current research.

MATERIALS AND METHODS

Constructs

pUASt-LSSmKate2, pUASt-mBeRFP and pUASt-NLSmBeRFP

LSSmKate2 and mBeRFP were individually amplified by PCR with specific primers from pLSSmKate2-N1 (Addgene plasmid #31867) and

Development (2022) 149, dev200495. doi:10.1242/dev.200495

LK1-MpEF1+mBeRFP+Nos-T35S-T (gift from F. Federici, Pontificia Universidad Católica de Chile, Santiago, Chile), and then cloned into the KpnI site of pUASt using In-Fusion technology (Clontech). The forward and reverse primers used to amplify LSSmKate2 were, respectively, GGCCGCGGCTCGAGGGTACCATGAGCGAGCTGATTAAGGAG and AAAGATCCTCTAGAGCTAATTAAGCTTGTGCCCCAGT. The forward primer used to amplify mBeRFP was GGCCGCGGCTCGAGGGTACCATGGTGTCTAAGGGCGA. The reverse primers used were AAAGATCCTCTAGAGTTAATTAAGTTTGTGCCCCAGT or AAAGATCCTCTAGAGTACCTTGCGCTTTTTCTTGGGAGCTCCCTCATTAAGTTTGTGCCCCAGT to generate, respectively, the cytoplasmic or nuclear version of mBeRFP.

p-mBeRFP and p-NLSmBeRFP

To generate these constructs, the same strategy described above was used. Briefly, the mBeRFP coding sequence was cloned into the KpnI site of phsp70, which was derived from the pUASt by removing UAS sequence.

pUASt-α-catenin-mBeRFP

This construct was carried out by amplifying α-catenin coding sequence from a pUAS-Dαcatenin-TagRFP (kindly provided by K. Sugimura, Kyoto University, iCeMS, Japan) then cloning in-frame with mBeRFP in the pUASt-mBeRFP plasmid digested with KpnI, using In-Fusion technology. Forward and reverse primers used to amplify α-catenin coding sequence were, respectively, GGCCGCGGCTCGAGGATGTTAAAACCTGATAAAATGGGCA and CCCTTAGACACCATGGCAACAGCGTCAGCAGGACT.

Drosophila stocks

Transgenic lines carrying UAS-LSSmKate2, UAS-mBeRFP, UAS-NLSmBeRFP and UAS-α-catenin-mBeRFP insertion at attP40 or attP2 landing sites were generated in this study by standard procedures using PhiC31/attB-mediated integration. Injections were performed by the CBI *Drosophila* facility (Toulouse, France).

ap^{md544}-Gal4 (BDSC_3041), pdm2-Gal4 (BDSC_49828), E-cad-GFP (BDSC_60584), UAS-α-catenin-GFP (BDSC_58787) were obtained from Bloomington *Drosophila* Stock Center (BDSC). sqh-$eGFP^{KI}$[29B] (named MyoII-GFP in this article) were previously described (Ambrosini et al., 2019). Dll^{EM212}-Gal4 and UAS-α-catenin-TagRFP were, respectively, gifts from G. Morata (Centro de Biología Molecular Severo Ochoa, Madrid, Spain) and K. Sugimura (Kyoto University, iCeMS, Japan).

Immunofluorescence

Imaginal leg and wing disks were dissected 2 h after pupae formation or at third instar larval stage in 1× PBS. Tissues were fixed in 4% paraformaldehyde for 20 min, then washed in PBS and mounted in Vectashield containing (or not) either DAPI or phalloidin rhodamine (Vector Laboratories). For Fig. 3G, samples were washed in 0.3% Triton X-100, 1% bovine serum albumin in PBS (BBT) after fixation and incubated overnight at 4°C with rat anti-E-cadherin antibody (Developmental Studies Hybridoma Bank, DCAD2) diluted at 1:50 in BBT. After washes in BBT, tissues were incubated with 1:200 anti-rat IgG 647 for 2 h at room temperature with 1:500 phalloidin TRITC (Fisher Scientific). Then, samples were washed in 0.3% Triton X-100 in PBS and mounted on slides in Vectashield with DAPI (Vector Laboratories).

Drosophila live samples

For live imaging, FRAP and laser ablation experiments (Figs 1D, 2A-E and 4B-C″) in leg tissue, imaginal leg disks were dissected from prepupae in Schneider medium supplemented with 15% fetal calf serum, 0.5% penicillin-streptomycin and 2 µg/ml 20-hydroxyecdysone (Sigma-Aldrich, H5142) and mounted on slides.

For live imaging of cell division and photobleaching experiments in wing tissue (Figs 2F,G and 4A; Fig. S2), imaginal wing disks were dissected from early third-instar larvae in Schneider's insect medium supplemented with 15% fetal calf serum, 0.5% penicillin-streptomycin and mounted on slides.

Confocal, spectral and random illumination microscopy

Images were acquired with a Zeiss LSM880 confocal microscope (Carl Zeiss) equipped with a 30 mW 405 nm diode laser, a 34.4 mW 458/488/514 nm argon multiline laser, a 13 mW 561 nm DPSS laser and a 3 mW 633 nm HeNe laser on a Zeiss Axio Observer microscope. The microscope was also fitted with Plan-Apochromat 40×/NA 1.3 Oil DIC UV-IR M27, 63× C-Apochromat NA 1.2 Water Corr (Fig. 2C,D, FRAP and laser ablation) and 40× C-Apochromat NA 1.2 Water Corr (Fig. 2A,B, live imaging and photobleaching assay) objectives. *z*-stacks were acquired using either the laser-scanning confocal mode or the spectral mode and the adapted illumination source. A linear unmixing process was performed following spectral acquisition to separate each fluorophore based on their spectra.

Fig. 3G was generated using three different tracks. MyoII-GFP and α-catenin-mBeRFP were imaged simultaneously (track 1) using a 458 nm laser with two emission windows (490-510 nm and 642-695 nm, respectively, for GFP and mBeRFP); nuclei (DAPI) and actin (Phalloidin-TRITC) were imaged in a second track using 405 nm and 561 nm lasers, and E-cadherin (Alexa 647) with a 633 nm laser in a third track.

Random illumination microscopy (RIM) was then performed using a home-made system that has been previously described (Mangeat et al., 2021). Images were acquired every 4 ms using an inverted microscope (TEi Nikon) equipped with a 100× magnification, 1.49 N.A. objective (CFI SR APO 100XH ON 1.49 Nikon) and Abbelight two sCMOS camera (ORCA-fusion, Hamamatsu) system band pass filters (Semrock): FF01-514/30-25 for GFP, FF01-630/92-25 for mBeRFP, Fast diode lasers (Oxxius) with wavelength centered at 445 nm (LBX 445 100 CSB OE) were used for the excitation of both GFP and mBeRFP. A spatial light phase binary modulator (QXGA fourth dimensions) was conjugated to the image plane to create speckle random illumination. Image reconstruction was then performed as previously detailed (Mangeat et al., 2021) with the upgraded version of AlgoRIM V1.2: https://github.com/teamRIM/tutoRIM.

Photobleaching experiments

Photobleaching was performed on the LSM880 confocal microscope. GFP and/or mBeRFP were excited simultaneously using the 458 nm laser source and photons were collected by GaAsP detectors. Images were acquired from imaginal wing disks every 6 min over 240 min (41 time frames).

FRAP experiments

FRAP was performed on the LSM880 confocal microscope described above. For FRAP experiments, GFP and/or mBeRFP were excited simultaneously using the 458 nm laser source, while TagRFP was excited with 561 nm, and photons were collected by GaAsP detectors. Photobleaching was set through the bleaching module provided with ZEN software. Briefly, the region of interest (ROI) was illuminated five times using a bleach dwell time of 0.60 µs/pixel with 100% 488 nm or 561 nm laser power. Images were acquired every 900 ms, ten times before bleaching and 100 times post-bleaching.

Laser ablation

Laser-ablation experiments were carried out using a pulsed DPSS laser (532 nm, pulse length 1.5 ns, repetition rate up to 1 kHz, 3.5 µJ/pulse) steered by a galvanometer-based laser scanning device (DPSS-532 and UGA-42, from Rapp OptoElectronic, Hamburg, Germany) and mounted on an LSM880 confocal microscope (Carl Zeiss). The microscope was fitted with a 63× C-Apochromat NA 1.2 Water Corr objective (Carl Zeiss). Photo-ablation of the apical junction was carried out in the focal plane by illuminating at 95-98% laser power for 500 ms. Time-lapse images were acquired using a 458 nm light source, every 370 ms, from 5 s before to at least 200 s after ablation, with a pixel size of 0.13 µm/pixel, and photons were collected in two emission windows (from 490 nm to 550 nm for eGFP and from 600 nm to 700 nm for mBeRFP).

Quantification

To assess the crosstalk, photobleaching or fluorescence intensity, the mean of fluorescence intensity was measured in the ROI using ImageJ (Figs 1G and 2B-G; Figs S1D, S2, S3D).

Development (2022) 149, dev200495. doi:10.1242/dev.200495

The crosstalk in classical laser-scanning mode between GFP and mBeRFP was calculated as the difference between the rate of eGFP emitted in the mBeRFP emission window when imaged at 458 nm with the spectral mode and the corresponding rate in the classical mode. The crosstalk in classical laser-scanning mode between mBeRFP and TRITC was calculated as the difference between the rate of mBeRFP emitted in the TRITC emission window when imaged at 561 nm with the spectral mode and the corresponding rate in the classical mode.

Vertex displacement was evaluated by kymograph using a home-made macro in ImageJ.

The analysis of the FRAP experiments was performed using a home-made macro in ImageJ based on the publication of Sidor et al. (2020). Briefly, fluorescence intensity (I) was measured in a ROI at the site of bleach and, to take into account general photobleaching, measures were normalized by a photobleaching correction factor ($C_{photobleaching}$) such as:

$$F_t = I_t \times C_{photobleaching\ t}, \quad (1)$$

with

$$C_{photobleaching\ t} = \frac{background\ intensity\ at\ t_0}{backgroung\ intensity\ at(t)}, \quad (2)$$

where t_0 corresponds to the time frame of the photobleaching.

Then, normalized measurements (F_t) were used to determine and plot the percentage of fluorescence recovery as follows:

$$F(t) = \frac{F_t - F_0}{F_{prebleach} - F_0}, \quad (3)$$

with

$$F_{prebleach} = avg\ F_{t-10\ to\ t-1}. \quad (4)$$

Finally, using Prism 8 (GraphPad) we modeled the recovery using the one-phase association equation ($a(1-e^{-kt})$) and extracted the mobile fraction (a, corresponding to the plateau) and the half time.

Statistical analysis

The normality and the variance of data sets was determined using Prism 8 (GraphPad). A two-tailed unpaired Student's t-test was used to assess the significance in Figs 1G, 2D,E and 3F, and Fig. S1D. A two-tailed paired Student's t-test was used in 3E.

Acknowledgements

We would like to thank Bruno Monier for his constructive comments on the manuscript and Thomas Mangeat, from the LITC platform, for his help on RIM experiments.

Competing interests

The authors declare no competing or financial interests.

Author contributions

Conceptualization: E.M.; Methodology: E.M.; Formal analysis: E.M.; Investigation: E.M.; Writing - original draft: E.M., M.S.; Writing - review and editing: E.M., M.S.; Visualization: E.M.; Supervision: M.S.; Funding acquisition: M.S.

Funding

M.S. is supported by grants from the Agence Nationale de la Recherche (ANR; PRC AAPG2021, CellPhy) and from the Fondation ARC pour la Recherche sur le Cancer (ARC; Programme Labélisé AAP2020, ARCPGA12020010001154_1591). Open access funding provided by Fondation ARC pour la Recherche sur le Cancer. Deposited in PMC for immediate release.

Peer review history

The peer review history is available online at https://journals.biologists.com/dev/lookup/doi/10.1242/dev.200495.reviewer-comments.pdf.

References

Ambrosini, A., Rayer, M., Monier, B. and Suzanne, M. (2019). Mechanical function of the nucleus in force generation during epithelial morphogenesis. *Dev. Cell* **50**, 197–211. doi:10.1016/j.devcel.2019.05.027

Antunes, M., Pereira, T., Cordeiro, J. V., Almeida, L. and Jacinto, A. (2013). Coordinated waves of actomyosin flow and apical cell constriction immediately after wounding. *J. Cell Biol.* **202**, 365-379. doi:10.1083/jcb.201211039

Bajar, B. T., Wang, E. S., Zhang, S., Lin, M. Z. and Chu, J. (2016). A guide to fluorescent protein FRET pairs. *Sensors (Basel)* **16**, 1488. doi:10.3390/s16091488

Boulina, M., Samarajeewa, H., Baker, J. D., Kim, M. D. and Chiba, A. (2013). Live imaging of multicolor-labeled cells in Drosophila. *Development* **140**, 1605-1613. doi:10.1242/dev.088930

Chalfie, M., Tu, Y., Euskirchen, G., Ward, W. W. and Prasher, D. C. (1994). Green fluorescent protein as a marker for gene expression. *Science* **263**, 802-805. doi:10.1126/science.8303295

Chudakov, D. M., Matz, M. V., Lukyanov, S. and Lukyanov, K. A. (2010). Fluorescent proteins and their applications in imaging living cells and tissues. *Physiol. Rev.* **90**, 1103-1163. doi:10.1152/physrev.00038.2009

Gorgidze, L. A., Oshemkova, S. A. and Vorobjev, I. A. (1998). Blue light inhibits mitosis in tissue culture cells. *Biosci. Rep.* **18**, 215-224. doi:10.1023/A:1020104914726

Heppert, J. K., Dickinson, D. J., Pani, A. M., Higgins, C. D., Steward, A., Ahringer, J., Kuhn, J. R. and Goldstein, B. (2016). Comparative assessment of fluorescent proteins for in vivo imaging in an animal model system. *Mol. Biol. Cell* **27**, 3385-3394. doi:10.1091/mbc.e16-01-0063

Icha, J., Weber, M., Waters, J. C. and Norden, C. (2017). Phototoxicity in live fluorescence microscopy, and how to avoid it. *BioEssays* **39**, 1700003. doi:10.1002/bies.201700003

Kasza, K. E., Farrell, D. L. and Zallen, J. A. (2014). Spatiotemporal control of epithelial remodeling by regulated myosin phosphorylation. *Proc. Natl. Acad. Sci. USA* **111**, 11732-11737. doi:10.1073/pnas.1400520111

Kogure, T., Karasawa, S., Araki, T., Saito, K., Kinjo, M. and Miyawaki, A. (2006). A fluorescent variant of a protein from the stony coral Montipora facilitates dual-color single-laser fluorescence cross-correlation spectroscopy. *Nat. Biotechnol.* **24**, 577-581. doi:10.1038/nbt1207

Mangeat, T., Labouesse, S., Allain, M., Negash, A., Martin, E., Guénolé, A., Poincloux, R., Estibal, C., Bouissou, A., Cantaloube, S. et al. (2021). Super-resolved live-cell imaging using Random Illumination Microscopy. *Cell Rep. Methods* **1**, 100009. doi:10.1016/j.crmeth.2021.100009

Piatkevich, K. D., Hulit, J., Subach, O. M., Wu, B., Abdulla, A., Segall, J. E. and Verkhusha, V. V. (2010a). Monomeric red fluorescent proteins with a large Stokes shift. *Proc. Natl. Acad. Sci. USA* **107**, 5369-5374. doi:10.1073/pnas.0914365107

Piatkevich, K. D., Malashkevich, V. N., Almo, S. C. and Verkhusha, V. V. (2010b). Engineering ESPT pathways based on structural analysis of LSSmKate red fluorescent proteins with large Stokes shift. *J. Am. Chem. Soc.* **132**, 10762-10770. doi:10.1021/ja101974k

Sahai, E., Wyckoff, J., Philippar, U., Segall, J. E., Gertler, F. and Condeelis, J. (2005). Simultaneous imaging of GFP, CFP and collagen in tumors in vivo using multiphoton microscopy. *BMC Biotechnol.* **5**, 14. doi:10.1186/1472-6750-5-14

Schott, S., Ambrosini, A., Barbaste, A., Benassayag, C., Gracia, M., Proag, A., Rayer, M., Monier, B. and Suzanne, M. (2017). A fluorescent toolkit for spatiotemporal tracking of apoptotic cells in living. *Development* **144**, 3840-3846. doi:10.1242/dev.149807

Shimomura, O., Johnson, F. H. and Saiga, Y. (1962). Extraction, purification and properties of aequorin, a bioluminescent protein from the luminous hydromedusan, Aequorea. *J. Cell. Comp. Physiol.* **59**, 223-239. doi:10.1002/jcp.1030590302

Sidor, C., Stevens, T. J., Jin, L., Boulanger, J. and Röper, K. (2020). Rho-kinase planar polarization at tissue boundaries depends on phospho-regulation of membrane residence time. *Dev. Cell* **52**, 364-378.e67. doi:10.1016/j.devcel.2019.12.003

Subach, O. M., Cranfill, P. J., Davidson, M. W. and Verkhusha, V. V. (2011). An enhanced monomeric blue fluorescent protein with the high chemical stability of the chromophore. *PLoS One* **6**, e28674. doi:10.1371/journal.pone.0028674

Thorn, K. (2017). Genetically encoded fluorescent tags. *Mol. Biol. Cell* **28**, 848-857. doi:10.1091/mbc.e16-07-0504

Wiedenmann, J., Oswald, F. and Nienhaus, G. U. (2009). Fluorescent proteins for live cell imaging: opportunities, limitations, and challenges. *IUBMB Life* **61**, 1029-1042. doi:10.1002/iub.256

Yang, J., Wang, L., Yang, F., Luo, H., Xu, L., Lu, J., Zeng, S. and Zhang, Z. (2013). mBeRFP, an improved large stokes shift red fluorescent protein. *PLoS ONE* **8**, e64849. doi:10.1371/journal.pone.0064849

Yonemura, S., Wada, Y., Watanabe, T., Nagafuchi, A. and Shibata, M. (2010). α-Catenin as a tension transducer that induces adherens junction development. *Nat. Cell Biol.* **12**, 533-542. doi:10.1038/ncb2055

Zimmermann, T., Rietdorf, J. and Pepperkok, R. (2003). Spectral imaging and its applications in live cell microscopy. *FEBS Lett.* **546**, 87-92. doi:10.1016/S0014-5793(03)00521-0

Zulueta-Coarasa, T. and Fernandez-Gonzalez, R. (2018). Dynamic force patterns promote collective cell movements during embryonic wound repair. *Nat. Phys.* **14**, 750-758. doi:10.1038/s41567-018-0111-2